



โครงการ

การเรียนการสอนเพื่อเสริมประสบการณ์

ชื่อโครงการ

การสังเคราะห์อนุภาคนาโนวานาเดียมไดออกไซด์ (VO_2)

ที่มีคุณสมบัติเทอร์โมโครมิก เพื่อประยุกต์ใช้งานในกระจกอัจฉริยะ

Synthesis of Vanadium dioxide (VO_2) nanoparticles for thermochromic applications

ชื่อนิสิต

นางสาวรัฐชนก จงประสิทธิ์

เลขประจำตัวนิต 6033432623

ภาควิชา

ฟิสิกส์

ปีการศึกษา

2563

คณะวิทยาศาสตร์ จุฬาลงกรณ์มหาวิทยาลัย

CHULALONGKORN UNIVERSITY

SENIOR PROJECT

2304449

**Synthesis of Vanadium dioxide
 VO_2 nanoparticles for
thermochromic applications**

Author:
Rattachanok Chongprasit

Advisor:
Salinporn Kittiwatanakul,
Ph.D

May 21, 2021

A report submitted to the Department of Physics of Chulalongkorn University in partial fulfillment of the requirements for the degree of Bachelor of Science in Physics Academic Year 2020

Project title Synthesis of Vanadium dioxide (VO_2) nanoparticles
for thermochromic applications

Author Rattachanok Chongprasit

Field of study Physics

Project Advisor Salinporn Kittiwatanakul, Ph.D.


Academic year 2020

This report is submitted to the Department of Physics, Faculty of Science, Chulalongkorn University, in partial fulfillment of the requirements for the degree of Bachelor of Science.

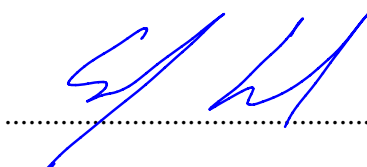
This report has been approved by the committee:


..... Chairman

Chatchai Srinitiwatwong, Ph.D.


..... Committee

Asst. Prof. Noravee Kanchanavatee, Ph.D.


..... Advisor

Salinporn Kittiwatanakul, Ph.D.

Project title Synthesis of Vanadium dioxide (VO_2) nanoparticles
for thermochromic applications

Author Rattachanok Chongprasit

Field of study Physics

Project Advisor Salinporn Kittiwatanakul, Ph.D.

Academic year 2020

Abstract

Vanadium dioxide (VO_2) has a metal-semiconductor phase transition at 68°C . This transition associates with the change of crystallographic structure from the monoclinic (M, $P21/c$, semiconductor) to the rutile (R, $P42/mnm$, metal). Abrupt changes in transmittance and reflectance in the Infrared region and electrical resistance also occur during the transition. This optical property can be used in energy-saving smart windows (automatically block heat). In this study, VO_2 nanoparticles have been fabricated by combusting the low-cost precursor solution consisting of NH_4VO_3 , $C_2H_6O_2$ and C_2H_5OH . Structural analysis of VO_2 was studied by X-ray diffraction (XRD) and Raman spectroscopy. Though XRD pattern are well corresponding to $VO_2(M)$, Raman results (grinded vs. non-grinded powder) demonstrate the same response as V_6O_{13} . After spin coating with polymer PMMA, the optical properties of VO_2 -based composited film was measured to be 70-90% of transmittance and $\approx 16\%$ of reflectance of 300-2,400 nm wavelength at the room temperature. The variation of transmittance are observed when the particle density is varied. However, there is no change or very little change of reflectance when sample are heated up to 90°C . This could lead to focus on synthesis process and Raman analysis that affect the optical properties at room temperature (semiconductor) and at 90°C (metal).

Keyword : Vanadium dioxide, monoclinic, rutile, XRD, Raman spectroscopy

Acknowledgement

Though a long road has been travelled thus far, I feel the journey has just begun. I do not know where the path will lead from here on, but I am ready for the next step.

This work was done in Department of Physics, Faculty of Science, Chulalongkorn University. First, I would like to very thank to my advisor, Ajarn Lin (Salinporn Kittiwatanakul, Ph.D) who always teach and support me for many things I do not understand. Next, I would like to express my sincere gratitude for both committees, Chatchai Srinithiwatwong, Ph.D and Asst. Prof. Noravee Kanchanavatee for their intention and guidance for making the completion of this project possible. UV-Vis-IR spectrophotometry has been important in my work, and I am very grateful to Asst. Prof. Sojiphong Chatraphorn, Ph.D and P' Luck, Boonyaluck Namnuan for the help and advices related to this experiment.

Lastly, I'd like to thank my parents and friends who have been nurturing, encouraging, and pushing me in the right path.

My best gratitude
Rattachanok Chongprasit

Contents

1	Introduction	1
1.1	Motivation	1
1.2	Project Objective	4
1.3	Expected Outcome	4
1.4	Project plan	5
1.5	List of Abbreviation and Symbols	6
2	Background and Theory	7
2.1	Structure and phase transition of VO_2	7
2.2	X-ray Diffraction (XRD)	8
2.2.1	Generation of X-rays	8
2.2.2	Bragg's law	9
2.2.3	Crystallography	10
2.3	Raman Spectroscopy	11
2.4	UV-Vis-IR spectrophotometry	12
2.4.1	Instrumentation	14
3	Methodology and Experiment	16
3.1	Synthesis of VO_2 nanoparticles	16
3.2	Preparation of thermochromic films	18
3.3	Phase confirmation by X-ray powder diffraction	18
3.4	Effect of particle size by Raman spectroscopy	19
3.5	Optical properties by UV-Vis-IR spectrophotometer	20
4	Results and Discussion	22
4.1	Analysis of XRD pattern of obtained black-blue powder	22
4.2	Effect of particle size by Raman spectroscopy	23
4.3	The optical properties of VO_2 composited films	25
4.3.1	Analysis of transmittance spectrum of VO_2 based films	25
4.3.2	Analysis of reflectance spectrum of VO_2 based films	27

5	Conclusions and Future works	32
5.1	Conclusions	32
5.2	Future work	33
5.2.1	Analysis of SEM images for the obtained VO_2	33
5.2.2	Determine the other phases of vanadium oxide	33
	Appendices	34
A	X-ray diffraction databases	35
A.1	Database of VO_2 (M)	35
A.2	Database of V_6O_{13}	40
A.3	Database of VEG	43
B	Raman scattering of V_6O_{13}	46
	Bibliography	49

List of Figures

1.1	Schematic of electrochromic smart window	2
1.2	Schematic of thermochromic smart window	2
2.1	Schematic of metal-semiconductor phase transition	8
2.2	Geometrical representation of Bragg's law	9
2.3	Absorption excitation of an electron	12
2.4	Incident light (I_0) passing through a sample that transmit light (I)	13
2.5	Specular (red) and diffuse (green) reflectance components . . .	14
2.6	Schematic of optical system in UV-Vis-IR spectrophotometer .	15
3.1	The flow chart of the solution preparation	17
3.2	(a) Combusting the mixture in evaporating dish directly (b) The black-blue powder before spin coating	17
3.3	Bruker's XRD D-8 Discover Instrument	19
3.4	Modular Raman spectrometer	19
3.5	Relative specular accessory	20
3.6	Mini hotplate with the thermocouple	21
4.1	a) XRD pattern of the black-blue powder b) XRD pattern of the VEG. Reproduced with the permission copyright 2016, Na- ture c) XRD pattern of monoclinic VO_2 Reproduced with the permission copyright 2016, Nature	23
4.2	Raman scattering of monoclinic VO_2	24
4.3	Compare the Raman spectrum between grinded powder and non-grinded powder	24
4.4	Raman scattering spectrum of a microcrystalline V_6O_{13} sample recorded at the room temperature	25
4.5	Transmittance spectrum from wavelength 300-2,400 nm at the room temperature	26
4.6	The relationships between electric current (I) and temperature (°C) of mini hotplate	28

4.7	The relationships between $T_{surface}$ ($^{\circ}\text{C}$) and T_{inner} ($^{\circ}\text{C}$) of mini hotplate	29
4.8	The reflectance spectra of sample (a)-(e) sample A-E and (f) sample D with heat sink silicone attached to mini hot plate at room temperature and 90°C	31

List of Tables

2.1	Three-dimensional lattice systems	10
3.1	List of samples in this work	18
4.1	The temperature of mini hot plate depends on applied current .	27

Chapter 1

Introduction

1.1 Motivation

The conservation of energy becomes nowadays the center of interest in many fields, in sustainable energy improvement which emphasize in the increase of energy efficiency to reduce the uses of energy as much as possible.

“Smart Window” has intelligent control which can reduce air-conditioning load to save energy as they are capable of modulating the solar radiation that passes through the window of the building. Besides window for office and homes, possible applications include automobile sunroof, sign and display, aircraft window, and spacecraft.

Electrochromic smart window (**Fig.1.1**) is controlled by the amount of voltage applied to the glass. Applying low voltage, the window is darken. Removing voltage, the window returns to lighten because electrons return to their original layers.[1]

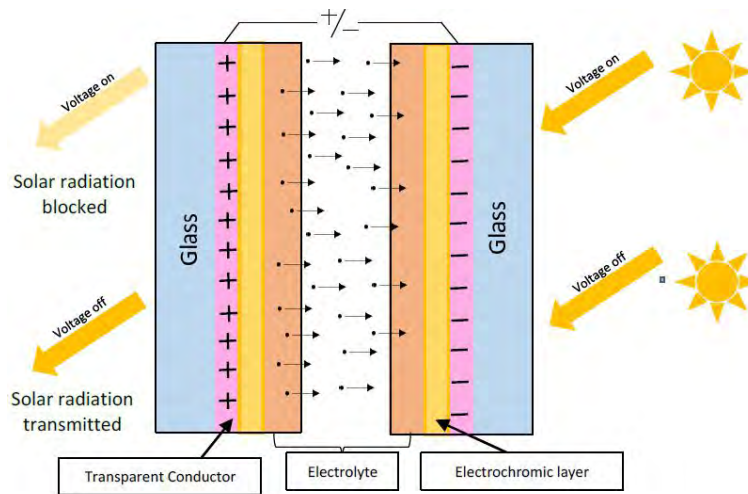


Figure 1.1: Schematic of electrochromic smart window [2]

Thermochromic smart window (**Fig.1.2**) differs from electrochromic smart window, which is triggered to dark state by heat instead of electricity. When the environmental temperature increases, the window turns to darken which blocks infrared.

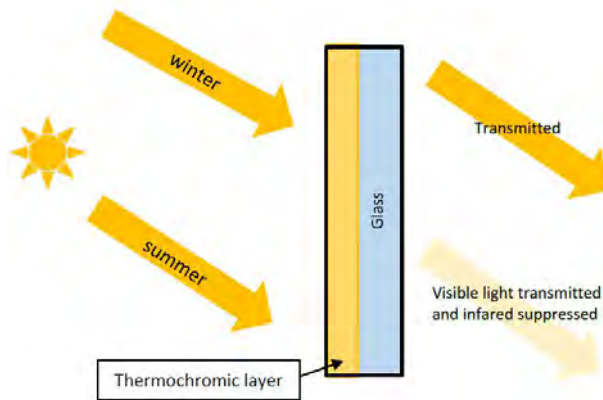


Figure 1.2: Schematic of thermochromic smart window [2]

Both, Electrochromic and thermochromic smart windows are the two ways to save the building energy. However, the high cost and complicated structure of electrochromic devices make them unaffordable to be mostly used. In contrast, thermochromic smart windows do not require additional energy to perform their function. This smart window could be produced by coating with some specific

materials on the glass substrate which can reflect the heat radiation from the sunlight.

In this case, thermochromic material could switch the reflection properties when the temperature changes across a specific temperature and also reduce the transmittance radiation passing through the building. Vanadium dioxide VO_2 is well-known as a glass coating material because it exhibit phase transition near room temperature around 68°C . [3] For practical application, VO_2 could be deposited on the glass substrate by physical or chemical process such as sputtering or chemical vapor deposition. These processes use the multi-step operation and time-consuming process.

Because of its unique metal-semiconductor phase transition characteristics, VO_2 has been widely used in photovoltaics, temperature sensor, smart window coating. [4]

There still remains another important challenge in improving the practical application of VO_2 based smart film for smart window application, which include low visible light transmission and high annealing temperature required to obtain pure phase $VO_2(\text{M})$. [4]

This work is expected to reduce the particle size which could increase the effective area by utilizing VO_2 nanoparticles for coating. VO_2 nanoparticles could potentially improve the problems of low visible light transmission, high phase transition temperature and low solar modulation rate of VO_2 continuous thin film in smart window applications. [4, 5] In addition, the simple synthesis of nanoparticles in this work will also shed light on the possibility of producing VO_2 nanoparticle thin film on flexible substrate such as thin plastic, polymer, or graphene because it does not require any high temperature annealing. [3]

1.2 Project Objective

1. To prepare thermochromic vanadium dioxide (VO_2) nanoparticles with a simple and low-cost method.
2. To determine the characteristic of VO_2 nanoparticles.
3. To study the transmittance spectrum of nanoparticle films of 300-2,400 nm wavelength with various spinning conditions and various particle density at room temperature.
4. To study the reflectance spectrum of 300-2,400 nm wavelength at room temperature and at 90°C for thermochromic application.

1.3 Expected Outcome

1. Gain knowledge and understand of synthesis process of VO_2 nanoparticles
2. Understand the instrument used such as Raman spectroscope, UV-Vis-IR spectrophotometer
3. Potentially gain good quality films to further explore with W-doping
4. Potential development for industrial scale production

1.4 Project plan

Action plan	2020							2021		
	Jun	Jul	Aug	Sep	Oct	Nov	Dec	Jan	Feb	Mar
1. Study the theoretical background and review existing literature	■	■								
2. Synthesis monoclinic VO ₂ nanoparticle and prepare the thermochromic film			■	■	■					
3. Determine the optical properties of the VO ₂ thin film					■	■	■			
4. Analysis of the experimental results							■	■		
5. Prepare the report and presentation						■	■	■	■	

1.5 List of Abbreviation and Symbols

3D	Three dimension
MST	Metal-semiconductor phase transition
PMMA	Poly(methyl methacrylate)
SEM	Scanning electron microscope
SNR	Signal to noise ratio
SPT	Structural phase transition
VEG	Vanadyl Ethylene Glycolate
XRD	X-ray powder diffraction
a	Lattice constant
a_1, a_2, a_3	Base vectors
c	Velocity of light
C	Concentration of sample
d_{hkl}	Inteplanar spacing
I_0	Incident light
I	Trasmit light
T_{MST}	Phase transition temperature
ε	Molar absorptivity
θ_B	Bragg angle
h	Planck's constant
λ	Wavelength

Chapter 2

Background and Theory

2.1 Structure and phase transition of VO_2

The atomic number of vanadium (V) is 23, and it is a transition metal. The electron configuration of vanadium is $[He]3d^34s^2$ so it partially filled 3d and 4s subshells. In addition to vanadium dioxide (VO_2), vanadium has many other stable oxides, such as vanadium monoxide (VO), vanadium trioxide (V_2O_3), and vanadium pentoxide (V_2O_5), as well as phases with other oxygen to vanadium ratios. V_2O_3 is an example of Magnéli phases with generic formula V_nO_{2n-1} . [6] Metal-semiconductor phase transition (MST) is observed in many of the vanadium oxides including V_2O_3 , V_3O_5 and VO_2 . [6] VO_2 has been the subject as it exhibits MST near room temperature around 68°C.

VO_2 has been the subject of intense research as it exhibits MST near room temperature around 68°C (340K). In addition to huge changes in the resistivity, optical properties are substantially modified during the transition, and a great variety of potential applications have been proposed which utilize MST in VO_2 . [7]

The metal-semiconductor transition in VO_2 is accompanied by a structural phase transition (SPT) from a low-temperature semiconductor phase to a high-temperature metallic phase. The phase that exhibits metallic behavior above the transition temperature has a tetragonal structure. Since the structure of the metallic phase resembles that of a rutile TiO_2 structure, the phase is known as R phase in **Fig.2.1**. In R phase, the vanadium atoms form a body-centered tetragonal lattice and are surrounded by an oxygen octahedron. [8] The insulating phase, which exists below phase transition temperature (T_{MST}), has a monoclinic structure, and it is known as M phase. Its unit cell is bigger than structure of the metallic phase.

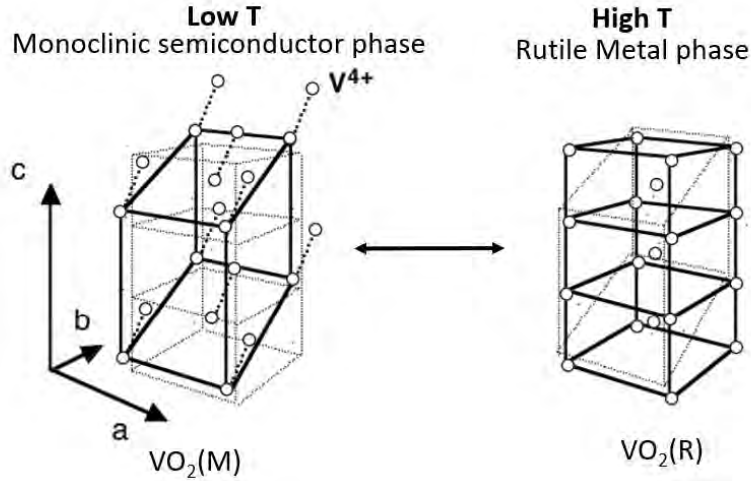


Figure 2.1: Schematic of metal-semiconductor phase transition [9]

The micromechanism of metal-semiconductor phase transition in VO_2 has been attached much attention, but there has been no MST model that explain all the experimental results. At the present, the explanation of the MST mechanism of VO_2 is mainly the debate[10] among the electron correlation driven Mott transition[11], the structure-driven Peierls transition[9] and the synergy between the two mechanisms.[12]

2.2 X-ray Diffraction (XRD)

2.2.1 Generation of X-rays

X-rays is an analytical technique primarily used for identification of a crystalline material and can provide information on unit cell dimensions because the wavelength of X-rays are the same scale as the distance between atom interaction. In observable diffraction depends on the phase difference between the scattered wave which is related to the atomic distance.

Synchrotron radiation and fluorescent X-ray emission are the main process for generation of X-rays. Synchrotron radiation emerges from the acceleration and deceleration of charged particles, such as electrons. When they travel through magnetic fields. Synchrotron radiation requires large facilities but produced radiation from a board range of spectrum with high intensity. In the other hand, Characteristic X-rays are generated when electron move to lower energy

that correspond to the difference of energy states (ΔE)

$$\Delta E = hf = \frac{hc}{\lambda} \quad (2.1)$$

where h is the Planck constant and c is the light velocity. For the electron to occupy this lower state, there must be an unfilled state. Otherwise the transition cannot occur because of the Pauli exclusion principle. Vacancies can be generated by bombardment of photons or particles which have high enough energy to remove an electron from the shell. To produce characteristic X-rays, electrons must be expelled from the innermost energy states requiring more energy.

2.2.2 Bragg's law

The X-ray diffraction can be described as Bragg's law where it has been assumed that all atoms in the unit cell are identical.[13] The summation can be calculated for Bravais lattices revealing that some reflections from planes (hkl) are forbidden since they yield a zero coefficient. These reflections, although predicted by Bragg's law, are thereby not observed. Bragg's law is presented as

$$2d_{hkl} \sin \theta_B = n\lambda \quad (2.2)$$

where θ_B is known as the Bragg angle, which gives the maximum intensity, n is a positive integer which represents the order of diffraction and d_{hkl} is the vector drawn from the origin to the plane (hkl) at a 90° angle. In diffractometers, the X-ray wavelength λ is fixed. The representation of Bragg's law is shown in **Fig.2.2**

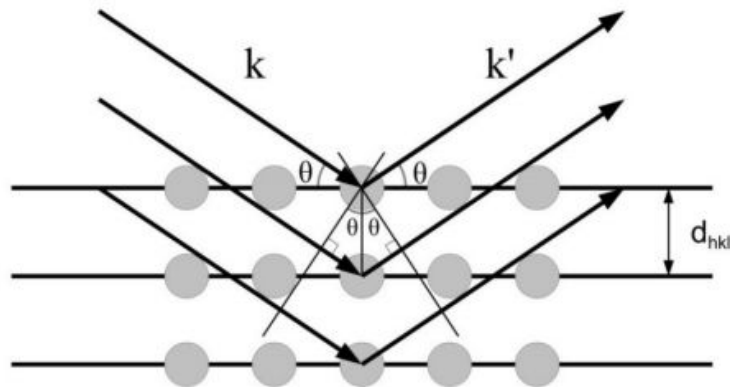


Figure 2.2: Geometrical representation of Bragg's law

So, we often consider the position of the diffraction peaks are determined by the distance between parallel planes of atoms which is the magnitude of vector d_{hkl} .

2.2.3 Crystallography

Unit cell is the smallest and symmetric cell which can be used to reproduce the whole crystal. The vectors forming the unit cell are called unit cell axes or crystal axes. The lengths of the vectors are called lattice constants. The unit cell is characterized by its lattice parameters comprising of the length of the vectors and angles between them.

Overall, 7 lattice systems based on the shape of the unit cell and 4 types of unit cells exist. Taking into account all the three-dimensional (3D) lattices which are symmetrically different, 14 called Bravais lattices exist. The 7 lattice systems and the corresponding lattice parameters are summarized in **Table 2.1**

Table 2.1: Three-dimensional lattice systems

Lattice System	Lattice Parameter		Bravis Lattices
	Crystal Axes	Angles	
Cubic	$a_1 = a_2 = a_3$	$\alpha = \beta = \gamma = 90^\circ$	P(Primitive)
			I(Body-centered)
			F(Face-centered)
Hexagonal	$a_1 = a_2 \neq a_3$	$\alpha = \beta = 90^\circ, \gamma = 120^\circ$	P(Primitive)
Monoclinic	$a_1 \neq a_2 \neq a_3$	$\alpha = \gamma = 90^\circ \neq \beta$	P(Primitive)
			C(Base-centered)
Orthorhombic	$a_1 \neq a_2 \neq a_3$	$\alpha = \beta = \gamma = 90^\circ$	P(Primitive)
			I(Body-centered)
			C(Base-centered)
			F(Face-centered)
Rhombohedral	$a_1 = a_2 = a_3$	$\alpha = \beta = \gamma \neq 90^\circ$	P(Primitive)
Tetragonal	$a_1 \neq a_2 \neq a_3$	$\alpha = \beta = \gamma = 90^\circ$	P(Primitive)
			I(Body-centered)
Triclinic	$a_1 \neq a_2 \neq a_3$	$\alpha \neq \beta \neq \gamma \neq 90^\circ$	P(Primitive)

α is angle between a_2 and a_3 , β is the angle between a_1 and a_3 , and γ is the angle between a_1 and a_2 .

It is a common convention to label a particular crystal plane using Miller indices (hkl). The three indexes (hkl) are found in the following. Miller indices for planes have been obtained, they can be used to calculate angles be-

tween planes as well as spacing between parallel planes. For the simplest and most symmetric structure, i.e. the cubic structure, the spacing between adjacent planes (hkl) is given by

$$d_{hkl} = \frac{a}{\sqrt{h^2 + k^2 + l^2}} \quad (2.3)$$

In this approach, we study the monoclinic system. It simplifies to

$$\frac{1}{d_{hkl}^2} = \frac{1}{\sin^2 \beta} \left(\frac{h^2}{a_1^2} + \frac{k^2 \sin^2 \beta}{a_2^2} + \frac{l^2}{a_3^2} - \frac{2hl \cos \beta}{a_1 a_3} \right) \quad (2.4)$$

2.3 Raman Spectroscopy

Raman spectroscopy is an analytical technique where scattered light is used to measure the vibrational energy modes of a sample. Raman spectroscopy can provide both chemical and structural information, as well as the identification of substance through their characteristic Raman "fingerprint". Raman spectroscopy shows this information through the detection of Raman scattering from the detection of Raman scattering from the sample.

When light is scattered by molecule, the oscillating electromagnetic field of a photon induces a polarisation of the molecular electron cloud which leaves the molecule in a higher energy state with the energy of the photon transferred to the molecule. This can be considered as the formation of a very short-lived complex between the photon and molecule which is commonly called the virtual state of the molecule. The virtual state is not stable and the photon is re-emitted almost immediately, as scattered light.[14]

Raman scattering occurs, which is an inelastic scattering process with a transfer of energy between the molecule and scattered photon. If the molecule gains energy from the photon during the scattering (excited to a higher vibrational level) then the scattered photon loses its energy and its wavelength which is called Raman scattering.[14]

The wavelength of the Raman scattered of the Raman scattered light will depend on the wavelength of excitation lighth, this makes the Raman scattering wavelength. The Raman scattered position is the inversion of Raman shift away from the excitation wavelength.[14]

2.4 UV-Vis-IR spectrophotometry

The wave-like nature of electromagnetic radiation is used in analytical technique to identify unknown substances and determine their optical characteristics. When a material is irradiated with electromagnetic waves, phenomena such as transmission, absorption, reflection, and scattering occur and the observed spectrum shows the interaction of wavelengths with objects of a discrete dimensions, such as atoms, molecules, and macromolecules.[15]

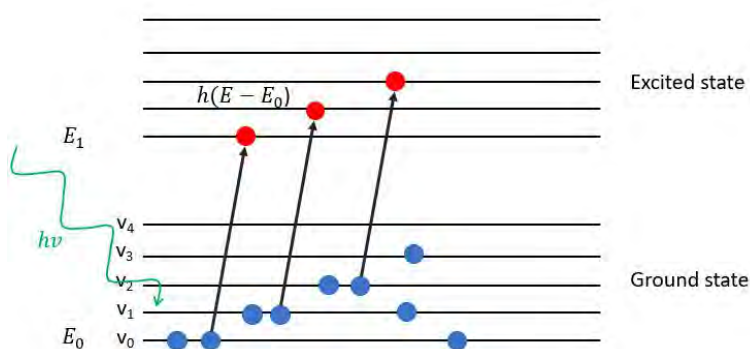


Figure 2.3: Absorption excitation of an electron [15]

Absorption occurs when the frequency of the incoming light is equal to the energy difference between a molecule's ground and excited states. The excitation of an electron from the ground state to the excited state is an electronic transition as shown in **Fig.2.3**.

The energy difference of each ground excited state pair corresponds to an absorption band. The relationship between the energy difference and wavelength is described by the Planck equation.

$$\Delta E = hf = \frac{hc}{\lambda} \quad (2.5)$$

where E is the energy required to promote an electron from the ground to excited state, h is Planck's constant, c is the speed of light, and λ is the wavelength. Planck's equation demonstrates that the less energy needed to excite the electrons, the longer the wavelength of the absorption band. The absorption bands are indicative of the molecular structure of the sample and will shift in wavelength and intensity depending on the molecular interactions and environmental conditions. These bands are typically broad and featureless due to the numerous molecular vibrational levels associated with the electronic energy levels.

UV-Vis-IR spectroscopy can be divided into ultraviolet, visible, and infrared regions of the spectrum depending on the wavelengths used. The ultraviolet region is typically measured from 180 to 400 nm, the visible light is 400 to 800 nm, and the infrared is 700 to 1,000 nm. Near-infrared light ranges from 700 to 3,000 nm.

Beer-Lambert Law

UV-Vis-IR spectrophotometer measures the transmittance or the amount of light transmitted through a sample by ratioing the intensity of the incident light (I_0) to the intensity of the transmitted light (I). [15]

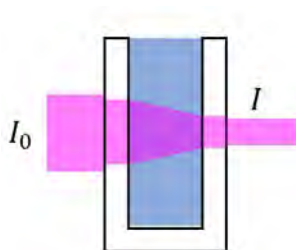


Figure 2.4: Incident light (I_0) passing through a sample that transmit light (I) [15]

Absorbance measurements are used to quantify concentration of sample by exploiting the Beer-Lambert Law that describes how light is attenuated based on the materials it passes through. The transmittance, and therefore the absorbance, are directly proportional to concentration of sample, C , molar absorptivity, ϵ , and cuvette pathlength, l . Taking the logarithm on both sides and transforming the formula,

$$-\log\left(\frac{I}{I_0}\right) = \epsilon \cdot C \quad (2.6)$$

The amount of light absorbed by the sample depends on the number of molecules interacted with. The more concentrated a sample is, the more molecules are present and the higher the absorbance. Likewise, the longer the pathlength of the cell, the greater the distance that the light travels through the sample, increasing the number of molecules interacted with and therefore the absorbance. To compare the absorbances of two solutions with either different concentrations or pathlengths, there needs to be a constant variable to normalize the data on. Additionally, to determine a sample's concentration by measuring absorbance, the cell pathlength and the strength of the electronic transition of the chromophore must be known. This constant or the probability of the electronic

transition occurring is the molar absorptivity. Since molecules have different electronic transitions of varying strengths, the molar absorptivity will vary depending on the transition being probed and is therefore wavelength dependent.

Aside from transmission and absorption, UV-Vis-IR spectroscopy can also measure the reflectance of a sample, or how effective a surface is in reflecting the total amount of incident light.[15]

Reflection occurs when light strikes a surface of material and causes a change in the direction of the light waves. There are two types of reflectance: specular and diffuse, where the sum of the two components is the total reflectance. Specular reflectance is light reflected at same angle as the incident beam and diffuse reflectance is light reflected off in many different directions, shown in **Fig.2.5**. [15]

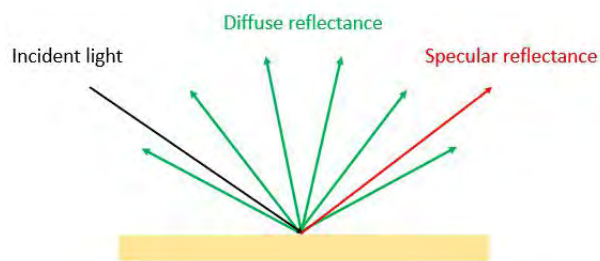


Figure 2.5: Specular (red) and diffuse (green) reflectance components [15]

2.4.1 Instrumentation

UV-visible spectrophotometer consists of a light source, a wavelength dispersive element, sample, and detector.[15]

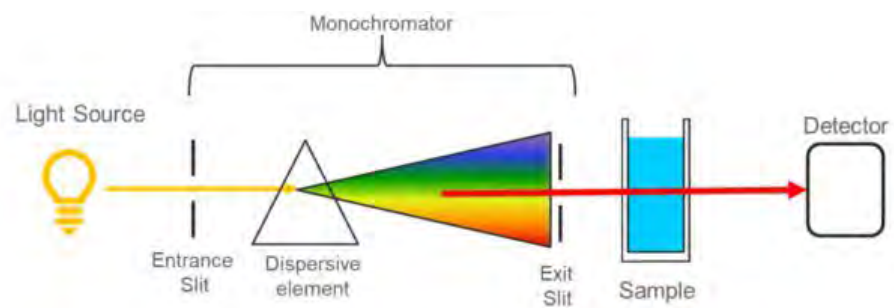


Figure 2.6: Schematic of optical system in UV-Vis-IR spectrophotometer [15]

Chapter 3

Methodology and Experiment

In this chapter we report on $VO_2(M)$ nanoparticle grown by combustion method and spin coated with PMMA as adhesive. XRD confirmed the VO_2 monoclinic phase before determining the effect of particle size with Raman spectrometer.

3.1 Synthesis of VO_2 nanoparticles

The following five steps are used for preparing the precursors, which is utilized before spin coating. They are shown in **Fig.3.1** and described in detail as follows.

1. Firstly, mixture of 1.0 g of powder of ammonium metavanadate (NH_4VO_3) and 37.5 ml of ethylene glycol in a beaker was heated to $70^\circ C$ for 30 minutes with 1,200 rpm magnetic stirring.
2. The transparent yellow solution was obtained after cooling at room temperature.
3. Then 37.5 ml of ethanol was added to the solution and the mixture was stirred for additional 30 minutes at room temperature.
4. The forming solution was poured in 285 ml-evaporating dish, then combusted directly with flame gun for 18 minutes in **Fig.3.2(a)**.
5. After the combustion, the black-blue powder in the inner wall of evaporating dish in **Fig.3.2(b)** was collected and divided to 2 packs : grinded and non-grinded powder .

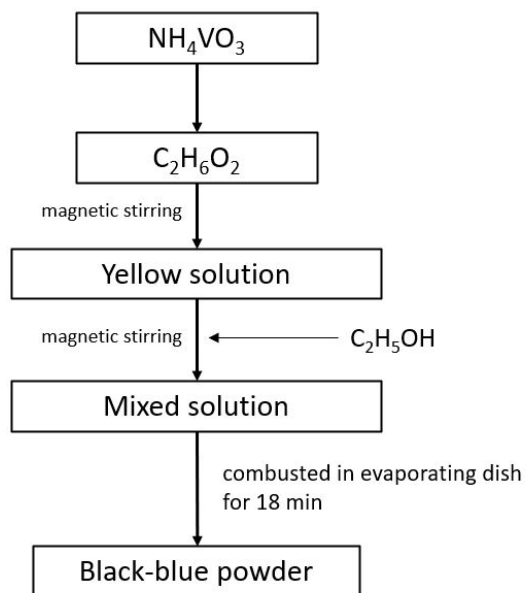


Figure 3.1: The flow chart of the solution preparation

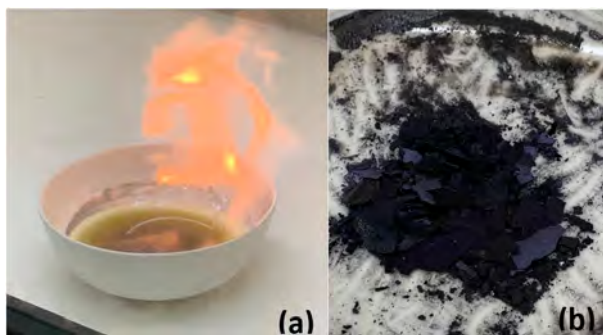


Figure 3.2: (a) Combusting the mixture in evaporating dish directly (b) The black-blue powder before spin coating

3.2 Preparation of thermochromic films

This work studies 2 variables.

- Spin speed
 - Particle density
1. Before spin coating, the glass slide substrate were pre-cleaned by spinning them with methanol and isopropanol (IPA) each time, then dried on the hot plate 90°C for 1 minute.
 2. The VO_2 (M) powder was mixed with the transparent PMMA and stirred for 5 minutes at room temperature.
 3. the solution was dropped onto steady 1x1 *inch*² glass substrate ensuring that the surface was covered completely and then started spinning at the different spin-coating speeds each time (2,000 rpm, 2,400 rpm and 3,300 rpm) for 20 seconds.
 4. After spin coating, the substrates were post-baked at 90°C for 1 minute, then cooled down at room temperature.

We selected five VO_2 thin film samples with various spin speeds and particle densities (**Table 3.1**).

Table 3.1: List of samples in this work

	Spin speed (rpm)	Particle density (g/ml of PMMA)
Sample A	3,300	0.1/10
Sample B	2,400	0.1/10
Sample C	2,000	0.1/10
Sample D	2,000	0.1/5
Sample E	2,400	0.1/5

3.3 Phase confirmation by X-ray powder diffraction

XRD data of the black-blue powder was collected on the Bruker's XRD D-8 Discover Instrument with $Cu-K\alpha$ (**Fig.3.3**)[16], Geology Laboratory, Chulalongkorn University. Sample was measured at a scanning rate of $1.0^\circ/s^{-1}$. The XRD pattern of VO_2 powder were recorded in the range $10^\circ-80^\circ$ using a step size of the 0.02° and a counting time 1 second per step.



Figure 3.3: Bruker's XRD D-8 Discover Instrument [16]

3.4 Effect of particle size by Raman spectroscopy

To confirm VO_2 monoclinic phase and to compare grinded vs. non-grinded powder. Raman spectroscope (**Fig.3.4**), 532 nm laser was used with 1,800 lines/mm grating. Scanning region is $100\text{-}700\text{ cm}^{-1}$ with the acquisition time of 60 seconds and 2 accumulations.



Figure 3.4: Modular Raman spectrometer [17]

3.5 Optical properties by UV-Vis-IR spectrophotometer

These samples were chosen such that there are with the same particle density or with substantially same spin speed. The spin speed given in **Table 3.1** were referred to the film thickness. So, the thickness of the VO_2 films may affect its optical properties.

To investigate the difference, we prepared VO_2 using the Perkin-Elmer spectrophotometer (Kit number B008-6703) in UV, visible light, Infrared over the wavelength of 300 to 2,400 nm, Semiconductor Physics Research Laboratory (SPRL), Chulalongkorn University.

For transmittance measurement, the sample spectra are normalised to the transmittance of transparent glass slide in UV, visible light, Infrared over the wavelength of 300 to 2,400 nm.

We measured transmittance spectra only at room temperature because we need to heat up the sample up to 90°C with mini hotplate which not designed for this sample holder. Therefore we will reported reflectance spectra at room temperature for the semiconductor phase and 90°C for the metallic phase.

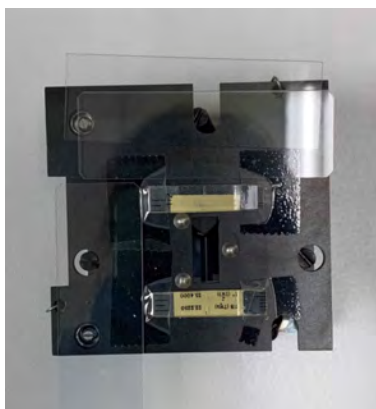


Figure 3.5: Relative specular accessory

For reflectance measurement, the sample are normalized to the reflectance of the mirror that put on the back of specular reflectance at 7.5° angle of incident in UV, visible light, Infrared over the wavelength of 300 to 2,400 nm[18] as shown in **Fig.3.5**.

Samples were placed at the back of specular. The sample heating was carried out using mini hot plate as shown in **Fig.3.6** with the thermocouple attached to the thermometer (TENMA, model 72-7715) for calibrating the appropriated current (I) to generate heat (at 90°C).



Figure 3.6: Mini hotplate with the thermocouple

Chapter 4

Results and Discussion

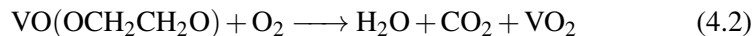
4.1 Analysis of XRD pattern of obtained black-blue powder

Monoclinic VO_2 can be formed via a combustion process. The XRD pattern of the black-blue powder in **Fig.4.1(a)**. It can be found that the XRD pattern of the participate matches well with the standard JCPDS card No.49-2497 in **Fig.4.1(b)** corresponding VEG (Vanadyl glycolate).

No peaks of the other phase and impurities are observed which indicate the pure VEG could be produced in the reaction as the following equation **Eq.(4.1)**



XRD pattern are well in agreement with the standard JCPDS card (No.43-1051) in **Fig.4.1(c)** corresponding to $VO_2(M)$. It means that after the black-blue powder reaction is $VO_2(M)$ as equation **Eq.(4.2)**



As is well known, the molecular structure is the a long chain.[19] Based on the reaction process and result obtained, it can be found that during the combustion, the chain-like VO_2 is formed.

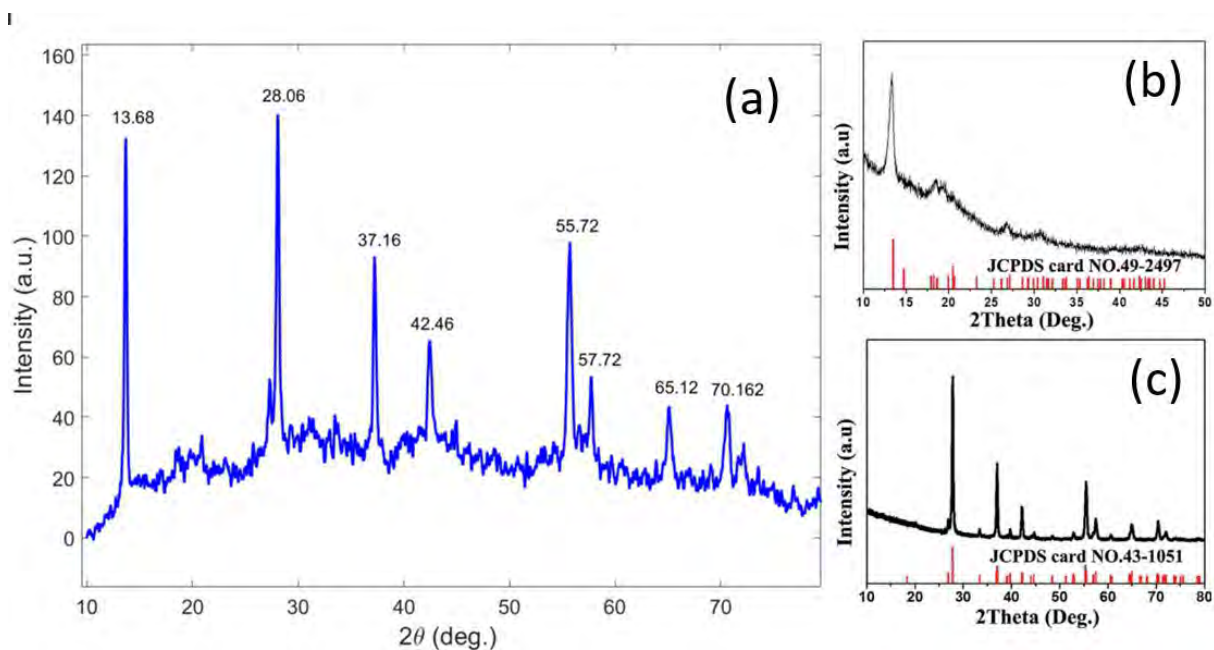


Figure 4.1: a) XRD pattern of the black-blue powder b) XRD pattern of the VEG. Reproduced with the permission copyright 2016, Nature c) XRD pattern of monoclinic VO_2 Reproduced with the permission copyright 2016, Nature

4.2 Effect of particle size by Raman spectroscopy

Commonly, the VO_2 (M) in **Fig.4.2** is associated with 18 Raman active vibrations. Raman modes have been found at 143, 192, 224, 261, 310, 340, 387, 499, 613 (with two shoulders at 590 and 665 cm^{-1}), and 824 cm^{-1} (a very weak line).[20]

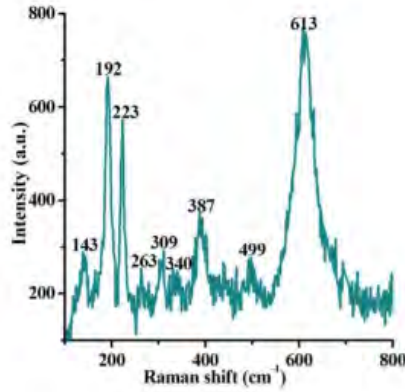


Figure 4.2: Raman scattering of monoclinic VO₂ [21]

Fig.4.3 shows variety of Raman spectra obtained with Modular Raman spectrometers from the different size of particles, which are not matched to monoclinic VO₂(M) in according with the previous report.

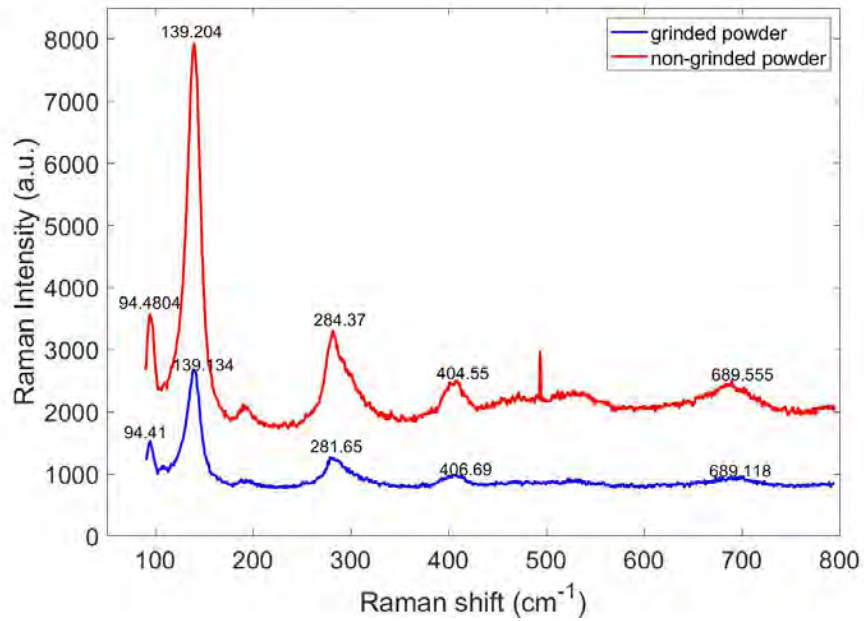


Figure 4.3: Compare the Raman spectrum between grinded powder and non-grinded powder

From the results, we can assume that particle size of black-blue powder does not affect the Raman spectra or the other phase of vanadium oxide is existent.

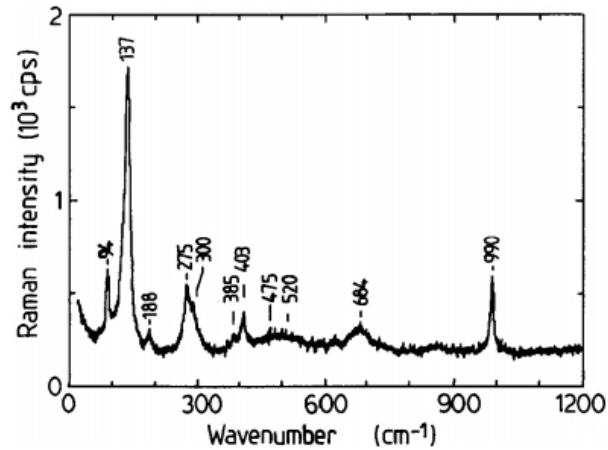


Figure 4.4: Raman scattering spectrum of a microcrystalline V_6O_{13} sample recorded at the room temperature [22]

The similarity between the Raman scattering of V_6O_{13} (Fig.4.4) and Fig.4.3 lead to the apparent contradiction between XRD and Raman results, since the monoclinic phase, observed in previous (Fig.4.1). Therefore, in our opinion the VO_2 (M) can be oxidized during stored in the air.

4.3 The optical properties of VO_2 composited films

4.3.1 Analysis of transmittance spectrum of VO_2 based films

The optical analysis results for each sample are shown in Fig.4.5. Transmittance demonstrates the thermochromic properties of each sample measured at room temperature between 300-2,400 nm wavelength.

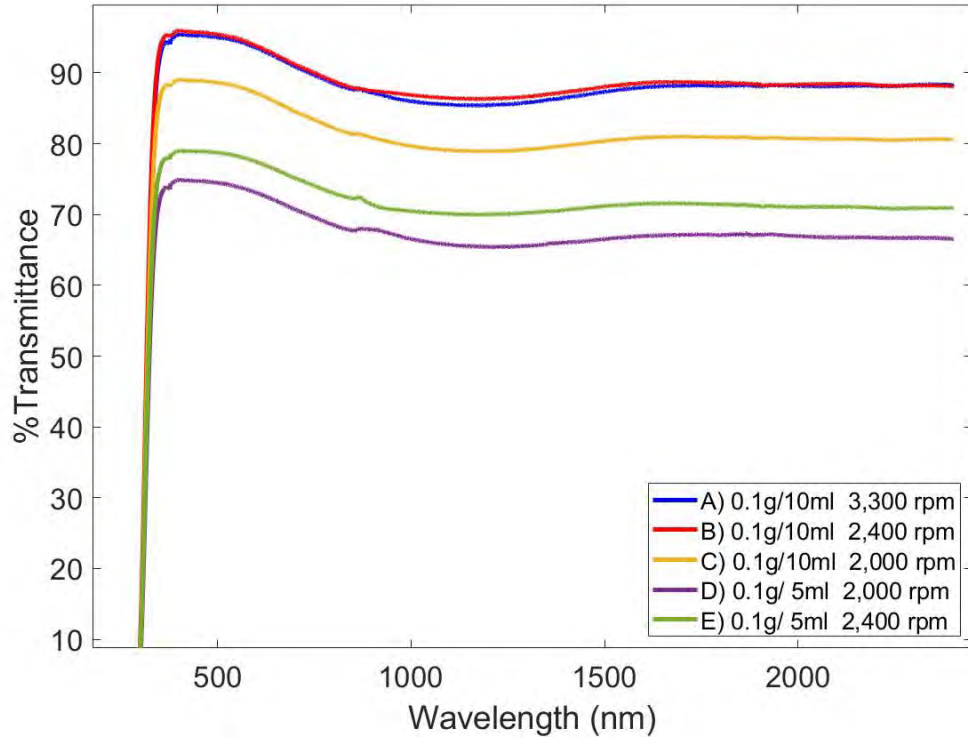


Figure 4.5: Transmittance spectrum from wavelength 300-2,400 nm at the room temperature

The transmittance of sample A was 95% which difference is not significant compared to sample B.

The others show a contrast change after reducing spin speed and increasing particle density. Though, the VO_2 film is thicker and denser, it exhibits lower transmittance and it clearly shows that all these exhibit high transmittance at room temperature following the typical semiconductor behavior, However it cannot be measured because the limitation of the heating setup transmittance spectrum at 90°C for metallic phase.

4.3.2 Analysis of reflectance spectrum of VO_2 based films

Furthermore, this optical results can be defined by the reflectance. The optical results exhibit the low reflectance of 300-2,400 nm wavelength at room temperature and 90°C of VO_2 flim on glass substrate directly attached to mini hotplate.

The reflectance of VO_2 films show similar trend of the temperature independent response as shown below (**Table 4.1**). In addition, the oscillation was obtained from optical reflectance at room temperature and at 90°C of each sample because of the glossy surface of Aluminium mini hot plate that cause the additional reflectance at its surface hence create the interference and the oscillation.

Table 4.1: The temperature of mini hot plate depends on applied current

Current (mA)	$T_{surface}(^{\circ}C)$	$T_{inner}(^{\circ}C)$
934	63.3	63.0
972	65.5	65.1
998	68.0	67.6
1008	70.1	69.8
1074	77.3	76.8
1117	78.4	77.8
1126	79.1	78.5
1225	84.6	84.0
1233	85.7	85.1
1264	86.4	85.4
1277	89.2	88.6
1303	90.3	89.6
1369	95.0	94.3
1382	99.9	100.1

The data plotted in **Fig.4.6** below was obtained by measuring temperature as a function of current. Over the range shown, temperature increase linearly with the current.

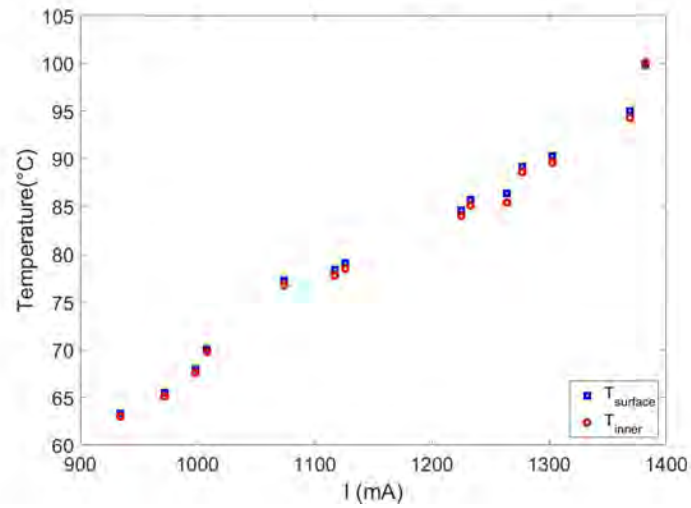


Figure 4.6: The relationships between electric current (I) and temperature (°C) of mini hotplate

The next plot (**Fig.4.7**) shows a relation between the temperature on the surface ($T_{surface}$) and the inner (T_{inner}) of mini hotplate. Two temperature reading of the thermometer will be taken to calibrate because the heated-up sample was placed on the surface of mini hotplate, so we need to temperature inside the mini hotplate for reference.

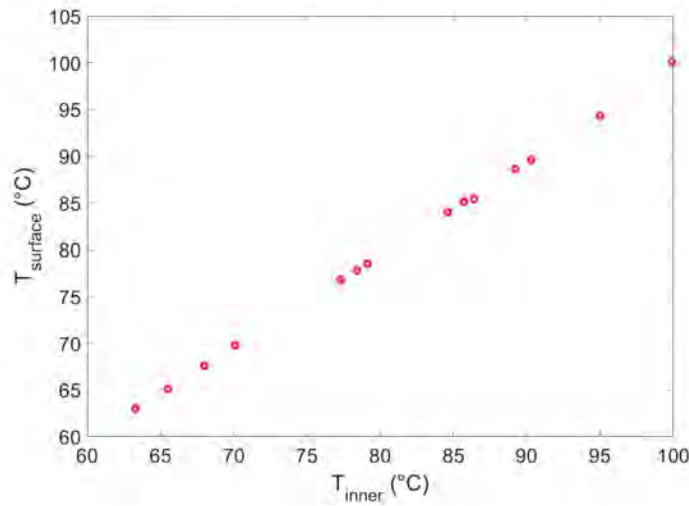


Figure 4.7: The relationships between $T_{surface}$ (°C) and T_{inner} (°C) of mini hotplate

An average temperature of 90°C of mini hotplate will required approximately 1.342 A of applied current.

Fig.4.8 (d) with highest particle density and spin speed (0.1g /5.0 ml of PMMA, 2,000 rpm) of sample D shows a little change of spectrum in Infrared region (700-1000 nm).

While using heat sink silicone to attach sample in **Fig.4.6(f)**, the results of sample D exhibit the different reflectance spectrum; The signal intensity for sample without mounting base (blue line) is higher than with mounting base (yellow line) at the room temperature because the lower reflected position could be eliminated any air gap and loss of light due to refraction.

In **Fig.4.8(d)** Aluminium hotplate amplified the signal, while using heat sink silicone reduced the signal and signal to noise ratio (SNR) occurred in **Fig.4.8 (f)**. However, it solves the oscillation problem from the interference from aluminium surface

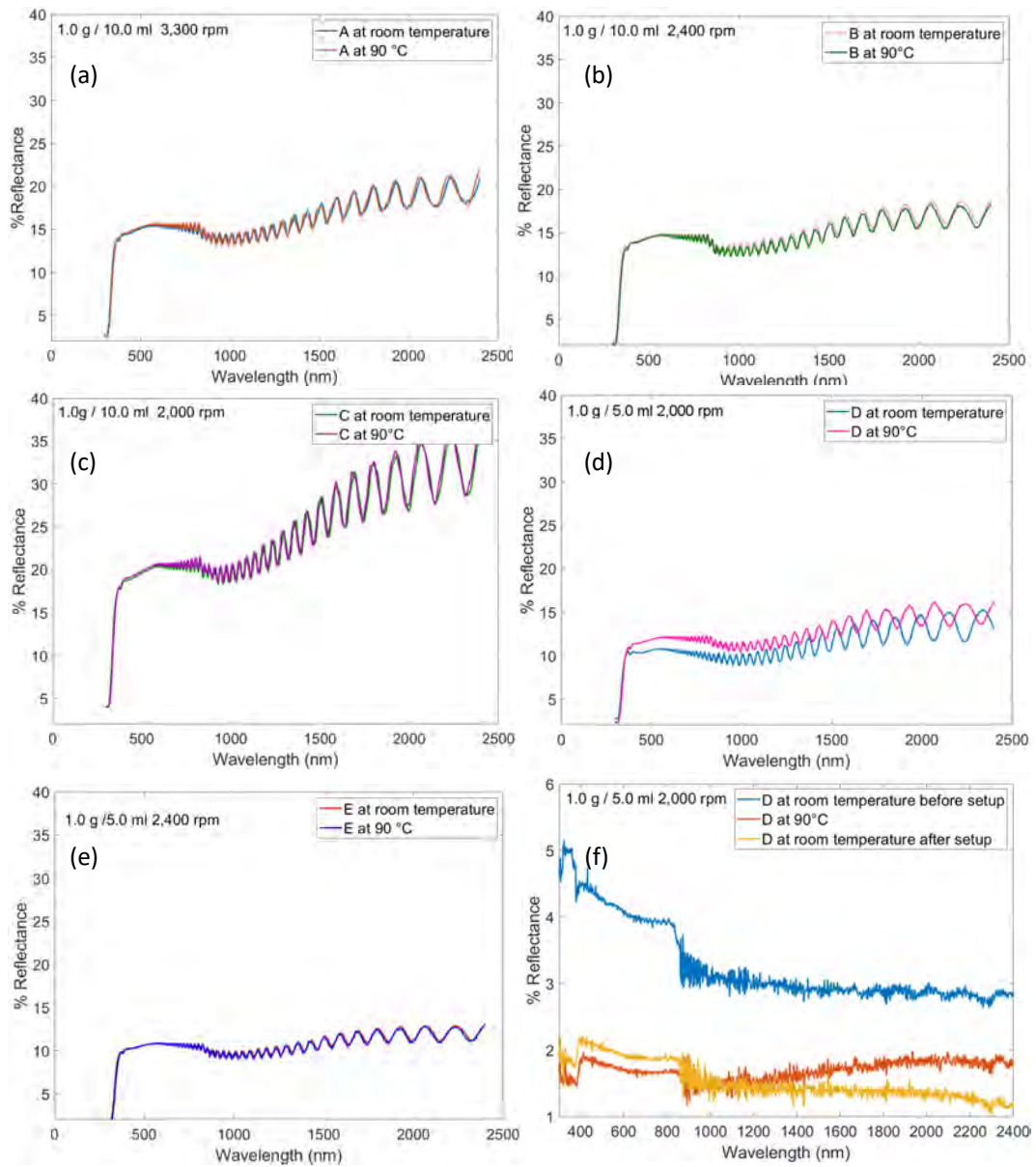


Figure 4.8: The reflectance spectra of sample (a)-(e) sample A-E and (f) sample D with heat sink silicone attached to mini hot plate at room temperature and 90°C

Chapter 5

Conclusions and Future works

5.1 Conclusions

In summary, monoclinic vanadium dioxide nanoparticles that confirmed by using XRD is successfully fabricated by combustion of precursor solution in the evaporating dish. The solution NH_4VO_3 , $C_2H_6O_2$ and C_2H_5OH are inexpensive and the period of the preparation and combustion is relatively short in air without the extra inert gas protection. But, we did not find any obvious features corresponding to VO_2 (M) by using Raman spectrometer. Moreover, the VO_2 based films made from VO_2 displays the excellent transmittance (up to 73%) and reflectance ($\approx 16\%$) which show semiconductor behavior. However, the reflectance spectrum at $90^\circ C$ do not show the switching characteristic, during the visible and infrared regions, respectively, except for sample D (0.1g/5 ml of PMMA, 2,000 rpm) that show little difference of reflectance ($\approx 10\%$) at $90^\circ C$. These results are quite encouraging, especially for the future plans.

5.2 Future work

5.2.1 Analysis of SEM images for the obtained VO_2

SEM images shall be taken to measure the size of the nanoparticles which was considered the friable structure, combustion method are introduced into this work to obtain VO_2 nanoparticles with narrow size distribution.

5.2.2 Determine the other phases of vanadium oxide

In previous study, the XRD results of synthesized $VO_2(M)$ nanoparticles by one-step pyrolysis with the same precursors at different time suggested that it can be found that the VEG complex still exist after 30-min pyrolysis, while diffraction peaks of the VEG complex gradually disappear when the time prolong to 35 minutes. High crystallinity and relatively pure phase $VO_2(M)$ powder is obtained after 60 minute. However, other phase of vanadium oxide (V_2O_5 , V_6O_{13} , V_3O_7) is also existent. It is not a result of surface oxidation, but rather partial energy surplus.[23]

The pyrolysis of VEG is an exothermic reaction and heat generated under the surface cannot dissipate at once. This leads to trace amounts of yellow vanadium peroxide powder which are only observed at the bottom of pyrolysis reactors. Part of V_2O_5 is also generated from the solvent–thermal process as mentioned above.[23]

According to the discussion of the previous research and Raman peaks in **Fig.4.3** corresponding to Raman scattering of V_6O_{13} , it could be one of the reasons that these samples does not exhibit the difference of reflectance in room temperature and at 90°C .

Another reason could be the particle density as seen result in **Fig.4.8**.

The following ideas lead to suggest future work:

1. Try to get rid of V_6O_{13} by varying burnt time
2. Try to increase the particle density
3. Study phase change of VO_x as function of stored time

Appendices

Appendix A

X-ray diffraction databases

A.1 Database of VO_2 (M)

Name and formula

Reference code: 00-043-1051
Compound name: Vanadium Oxide
PDF index name: Vanadium Oxide
Empirical formula: O₂V
Chemical formula: VO₂

Crystallographic parameters

Crystal system: Monoclinic
Space group: P21/c
Space group number: 14
a (Å): 5.7517
b (Å): 4.5378
c (Å): 5.3825
Alpha (°): 90.0000
Beta (°): 122.6400
Gamma (°): 90.0000
Calculated density (g/cm³): 4.66
Volume of cell (10⁶ pm³): 118.30
Z: 4.00
RIR: 3.25

Subfiles and Quality

Subfiles: Alloy, metal or intermetallic
Corrosion
Inorganic
Quality: Calculated (C)

Comments

Creation Date: 01/01/1970
Modification Date: 01/01/1970
Calculation of diffractometer peak intensities done with MICRO-POWD v. 2.2 (D. Smith and K. Smith) using default instrument broadening function (NBS Table), diffracted beam monochromator polarization correction, and atomic scattering factors corrected for anomalous dispersion. Cell parameters from Longo, J., *Acta Chem. Scand.* **24**, 420 (1970). Atomic positions from same source: V in 4e with x=0.23947, y=0.97894, z=0.02646, O(1) in 4e with x=0.10616, y=0.21185, z=0.20859, O(2) in 4e with x=0.40051, y=0.70258, z=0.29884
Isotropic thermal parameters also from Longo: V, B=0.299; O(1), B=0.396; O(2), B=0.441. Intensity threshold for <1=0.1%
Additional Patterns: See 9-142 for experimental data.

References

Primary reference: Grier, D., McCarthy, G., North Dakota State University, Fargo, North Dakota, USA., *JCDD Grant-in-Aid*, (1991)

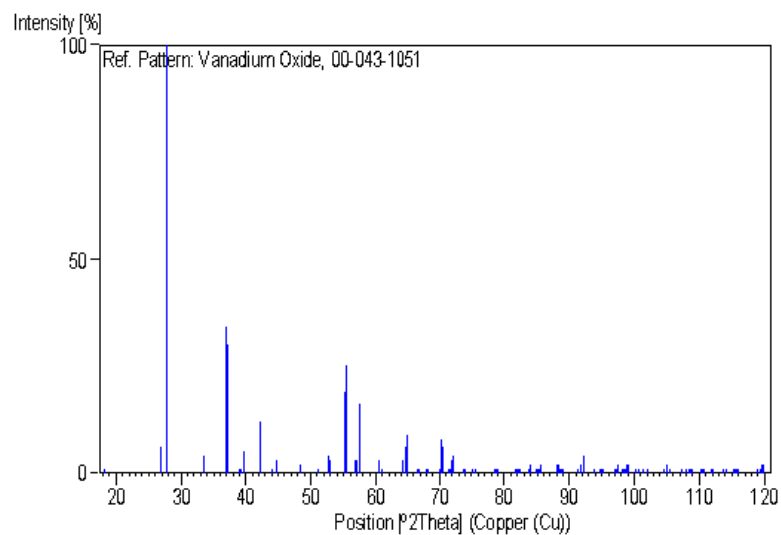
Unit cell: Longo, J., Kierkegaard, P., *Acta Chem. Scand.*, 24, 420, (1970)**Peak list**

No.	h	k	l	d [Å]	2Theta[deg]	I [%]
1	1	0	0	4.84300	18.304	1.0
2	-1	1	1	3.31600	26.865	6.0
3	0	1	1	3.20700	27.796	100.0
4	-1	0	2	2.68140	33.390	4.0
5	-2	0	2	2.43460	36.890	14.0
6	-2	1	1	2.42890	36.980	34.0
7	2	0	0	2.42200	37.089	30.0
8	-1	1	2	2.30880	38.979	1.0
9	1	1	1	2.30030	39.129	1.0
10	0	2	0	2.26770	39.715	5.0
11	-2	1	2	2.14560	42.079	12.0
12	2	1	0	2.13640	42.269	11.0
13	-1	2	1	2.05560	44.016	1.0
14	0	2	1	2.02800	44.647	3.0
15	-3	0	2	1.87800	48.431	2.0
16	-2	2	1	1.78130	51.245	1.0
17	-3	1	2	1.73530	52.706	1.0
18	-1	2	2	1.73190	52.817	4.0
19	1	2	1	1.72850	52.929	3.0
20	1	0	2	1.72610	53.009	1.0
21	-2	1	3	1.66060	55.274	19.0
22	2	2	0	1.65570	55.452	25.0
23	2	1	1	1.65290	55.554	22.0
24	-1	1	3	1.61820	56.852	3.0
25	3	0	0	1.61400	57.013	3.0
26	0	2	2	1.60340	57.425	16.0
27	-3	1	3	1.52840	60.529	3.0
28	3	1	0	1.52110	60.850	1.0
29	-3	2	2	1.44670	64.343	2.0
30	-3	2	1	1.44420	64.468	3.0
31	-4	0	2	1.43790	64.784	6.0
32	0	3	1	1.43420	64.972	9.0
33	-2	2	3	1.40300	66.602	1.0
34	2	2	1	1.39790	66.877	1.0
35	-1	2	3	1.37680	68.040	1.0
36	1	2	2	1.37380	68.209	1.0
37	-2	0	4	1.34080	70.130	1.0
38	-2	3	1	1.33870	70.257	8.0
39	2	0	2	1.33420	70.529	6.0
40	-3	0	4	1.32070	71.359	1.0
41	-1	3	2	1.31750	71.559	1.0
42	3	2	0	1.31540	71.691	1.0
43	-4	1	3	1.31410	71.773	3.0
44	-4	1	1	1.31000	72.033	4.0
45	-2	1	4	1.28540	73.635	1.0
46	2	3	0	1.28290	73.802	1.0
47	2	1	2	1.28000	73.997	1.0
48	-1	0	4	1.26500	75.025	1.0
49	0	3	2	1.25780	75.529	1.0
50	-4	0	4	1.21740	78.505	1.0
51	1	1	3	1.21560	78.644	1.0
52	-4	2	2	1.21450	78.729	1.0
53	4	0	0	1.21080	79.017	1.0
54	-3	3	2	1.17800	81.673	1.0

55	-3	3	1	1.17690	81.766	1.0
56	-4	1	4	1.17590	81.850	1.0
57	-4	2	1	1.17170	82.207	1.0
58	4	1	0	1.16990	82.361	1.0
59	-2	2	4	1.15410	83.741	1.0
60	2	3	1	1.15120	84.000	2.0
61	2	2	2	1.15010	84.098	2.0
62	-3	2	4	1.14180	84.852	1.0
63	-5	0	2	1.14030	84.990	1.0
64	-1	3	3	1.13930	85.082	1.0
65	1	3	2	1.13760	85.239	1.0
66	3	2	1	1.13670	85.323	1.0
67	0	4	0	1.13440	85.537	2.0
68	0	0	4	1.13310	85.659	2.0
69	-5	1	3	1.10750	88.139	2.0
70	-3	3	3	1.10660	88.229	1.0
71	-1	2	4	1.10490	88.400	2.0
72	3	3	0	1.10380	88.511	1.0
73	1	2	3	1.10270	88.623	1.0
74	0	4	1	1.10050	88.847	1.0
75	0	1	4	1.09940	88.959	1.0
76	-5	0	4	1.07720	91.302	1.0
77	-4	2	4	1.07280	91.784	2.0
78	0	3	3	1.06890	92.216	3.0
79	4	2	0	1.06820	92.294	4.0
80	-2	4	1	1.05530	93.762	1.0
81	-3	1	5	1.04710	94.724	1.0
82	-1	4	2	1.04480	94.999	1.0
83	-5	1	1	1.04400	95.095	1.0
84	-4	3	2	1.04220	95.311	1.0
85	-2	1	5	1.02860	96.987	1.0
86	2	4	0	1.02730	97.151	1.0
87	2	1	3	1.02490	97.456	2.0
88	-5	2	3	1.02010	98.072	1.0
89	-5	2	2	1.01890	98.228	1.0
90	-4	1	5	1.01810	98.332	1.0
91	-4	3	3	1.01660	98.528	1.0
92	-4	3	1	1.01460	98.790	2.0
93	0	2	4	1.01370	98.909	1.0
94	4	1	1	1.01230	99.094	2.0
95	-2	3	4	1.00340	100.294	1.0
96	2	3	2	1.00060	100.679	1.0
97	-3	3	4	0.99510	101.446	1.0
98	1	0	4	0.99110	102.013	1.0
99	-5	2	4	0.97310	104.669	1.0
100	-3	4	2	0.97100	104.991	1.0
101	-3	4	1	0.97020	105.114	2.0
102	1	3	3	0.96880	105.331	1.0
103	3	2	2	0.96790	105.471	1.0
104	2	4	1	0.95590	107.382	1.0
105	-5	1	5	0.95230	107.974	1.0
106	-1	4	3	0.94900	108.524	1.0
107	-4	3	4	0.94840	108.625	1.0
108	1	4	2	0.94800	108.692	1.0
109	5	1	0	0.94730	108.810	1.0
110	-6	0	4	0.93900	110.238	1.0
111	-6	1	3	0.93790	110.431	1.0
112	-6	0	2	0.93670	110.642	1.0
113	-3	4	3	0.92990	111.863	1.0
114	3	4	0	0.92820	112.174	1.0

115	-6	1	4	0.91950	113.804	1.0
116	-6	1	2	0.91740	114.208	1.0
117	-5	3	3	0.91140	115.383	1.0
118	-5	3	2	0.91060	115.543	1.0
119	-1	2	5	0.90980	115.703	1.0
120	1	2	4	0.90820	116.024	1.0
121	-3	0	6	0.89390	119.023	1.0
122	-4	0	6	0.89260	119.307	1.0
123	-1	5	1	0.89210	119.417	1.0
124	5	2	0	0.89070	119.726	2.0
125	0	5	1	0.88990	119.903	2.0

Stick Pattern



A.2 Database of V_6O_{13}

Date: 14/05/2021 Time: 9:16:41 AM

File: 00-025-1251

User: Mayur

Name and formula

Reference code: 00-025-1251
Compound name: Vanadium Oxide
PDF index name: Vanadium Oxide
Empirical formula: $O_{13}V_6$
Chemical formula: V_6O_{13}

Crystallographic parameters

Crystal system: Monoclinic
Space group: P21/a
Space group number: 14
a (Å): 11.9600
b (Å): 3.7130
c (Å): 10.0700
Alpha (°): 90.0000
Beta (°): 100.9000
Gamma (°): 90.0000

Volume of cell (10^6 pm^3): 439.12

RIR: -

Status, subfiles and quality

Status: Marked as deleted by ICDD
Subfiles: Alloy, metal or intermetallic
Inorganic
Quality: Indexed (I)

Comments

Creation Date: 01/01/1970
Modification Date: 01/01/1970
Deleted Or Rejected By: Deleted by 27-1318.

References

Primary reference: Kawada, et al., *J. Less-Common Met.*, **32**, 171, (1973)

Peak list

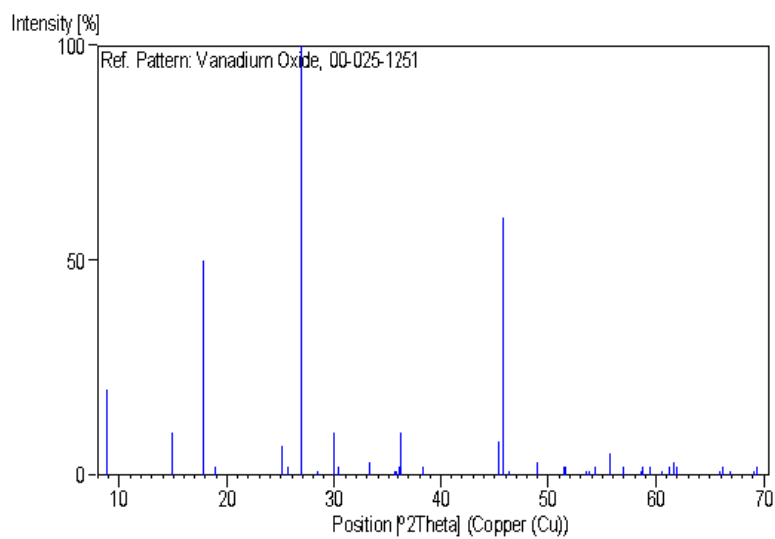
No.	h	k	l	d [Å]	2Theta[deg]	I [%]
1	0	0	1	9.96000	8.871	20.0
2	2	0	0	5.91000	14.978	10.0
3	0	0	2	4.97000	17.832	50.0
4	2	0	1	4.70000	18.866	2.0
5	1	1	0	3.55000	25.064	7.0
6	0	1	1	3.48000	25.577	2.0
7	0	0	3	3.31000	26.914	100.0

All the best

1 Of 3

8	-2	0	3	3.14000	28.401	1.0
9	-4	0	1	2.97800	29.982	10.0
10	4	0	0	2.94000	30.378	2.0
11	-3	1	0	2.69600	33.204	3.0
12	3	1	1	2.51800	35.627	1.0
13	-3	1	2	2.50900	35.759	1.0
14	-1	1	3	2.48500	36.116	2.0
15	0	0	4	2.47100	36.328	10.0
16	4	0	2	2.34200	38.405	2.0
17	-6	0	1	1.99600	45.402	8.0
18	0	0	5	1.97700	45.863	60.0
19	6	0	0	1.95900	46.309	1.0
20	0	2	0	1.85700	49.015	3.0
21	2	0	5	1.77600	51.409	2.0
22	2	2	0	1.77100	51.564	2.0
23	6	0	2	1.71300	53.446	1.0
24	1	2	2	1.70100	53.854	1.0
25	1	1	5	1.68700	54.337	2.0
26	0	0	6	1.64900	55.697	5.0
27	0	2	3	1.61700	56.898	2.0
28	-4	2	1	1.57500	58.560	1.0
29	-4	0	6	1.57000	58.765	2.0
30	-7	1	1	1.55300	59.472	2.0
31	-1	1	6	1.52800	60.546	1.0
32	4	0	5	1.51300	61.211	2.0
33	3	1	5	1.50400	61.617	3.0
34	-3	1	6	1.49600	61.982	2.0
35	-7	1	4	1.41500	65.965	1.0
36	6	0	4	1.41100	66.176	2.0
37	-6	0	6	1.39800	66.871	1.0
38	-6	2	1	1.35900	69.057	1.0
39	0	2	5	1.35300	69.407	2.0

Stick Pattern



A.3 Database of VEG

Date: 14/05/2021 Time: 9:17:59 AM

File: 00-025-1251

User: Mayur

Name and formula

Reference code: 00-049-2497
Compound name: Vanadyl ethylene glycolate
PDF index name: Vanadyl ethylene glycolate
Empirical formula: $C_2H_4O_3V$
Chemical formula: $C_2H_4O_3V$
Second chemical formula: $VO(C_2H_4O_2)$

Crystallographic parameters

Crystal system: Monoclinic
Space group: $C2/c$
Space group number: 15
a (Å): 9.2710
b (Å): 9.7350
c (Å): 9.9180
Alpha (°): 90.0000
Beta (°): 106.1110
Gamma (°): 90.0000

Calculated density (g/cm³): 1.96
Volume of cell (10⁶ pm³): 859.98
Z: 8.00

RIR: -

Subfiles and Quality

Subfiles: Organic
Quality: Star (S)

Comments

Color: Light purple
Creation Date: 01/01/1970
Modification Date: 01/01/1970
Sample Preparation: Prepared from LiOH and V_2O_5 (1:2 molar ratio) in ethylene glycol solution at hydrothermal conditions (Teflon-lined Parr reactor at 200 C for 2 days)
Temperature of Data Collection: Pattern taken at 23(1) C
Color: Light purple
The crystal structure refined from full profile powder data: Atom x/a y/b z/c B(is/eq) N V -0.0165(5)
.1239(4) .0917(5) .86(7) 8 C1 .271(3) .030(2) .270(3) 4.4(8) 8
C2 .279(3) .016(2) .132(2) 3.4(8) 8 O1 -0.115(11) .2673(12) .0192
(11) 1.3(3) 8 O2 .143(2) .1002(11) .2785(13) 1.9(4) 8 O3 .1286
(14) .0232(14) .032(2) 2.3(4) 8.

References

Primary reference: Whittingham, M., Zavalij, P., Inst. for Materials Research & Chemistry Dept., SUNY,

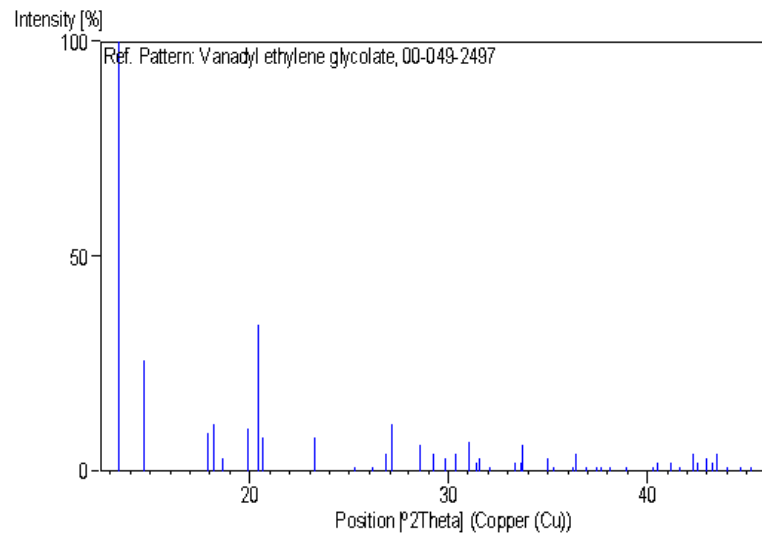
All the best

1 Of 3

Peak list

No.	h	k	l	d [Å]	2Theta[deg]	I [%]
1	1	1	0	6.57239	13.461	100.0
2	1	1	-1	6.01662	14.711	26.0
3	1	1	1	4.95813	17.875	9.0
4	0	2	0	4.86820	18.208	11.0
5	0	0	2	4.76444	18.608	3.0
6	2	0	0	4.45660	19.907	10.0
7	0	2	1	4.33653	20.464	34.0
8	1	1	-2	4.29892	20.645	8.0
9	2	0	-2	3.82523	23.235	8.0
10	1	1	2	3.52777	25.225	1.0
11	0	2	2	3.40516	26.149	1.0
12	2	2	-1	3.32293	26.808	4.0
13	2	2	0	3.28636	27.112	11.0
14	1	1	-3	3.11930	28.594	6.0
15	1	3	0	3.04868	29.271	4.0
16	1	3	-1	2.98713	29.888	3.0
17	3	1	-1	2.94175	30.360	4.0
18	2	0	2	2.87920	31.036	7.0
19	3	1	0	2.84224	31.450	2.0
20	1	3	1	2.82830	31.609	3.0
21	3	1	-2	2.78666	32.094	1.0
22	1	3	-2	2.68546	33.338	2.0
23	0	2	3	2.66219	33.638	2.0
24	1	1	3	2.65552	33.725	6.0
25	2	2	-3	2.55980	35.026	3.0
26	3	1	1	2.54091	35.295	1.0
27	2	2	2	2.47798	36.222	1.0
28	3	1	-3	2.46685	36.391	4.0
29	0	4	0	2.43354	36.907	1.0
30	1	1	-4	2.40135	37.420	1.0
31	0	0	4	2.38494	37.687	1.0
32	0	4	1	2.35813	38.132	1.0
33	1	3	-3	2.31166	38.929	1.0
34	3	3	-1	2.23719	40.280	1.0
35	4	0	0	2.22712	40.470	2.0
36	3	3	0	2.19152	41.157	2.0
37	0	4	2	2.16631	41.658	1.0
38	0	2	4	2.13558	42.286	4.0
39	3	1	-4	2.12475	42.512	2.0
40	1	1	4	2.10269	42.980	3.0
41	4	2	-1	2.08986	43.257	2.0
42	2	2	3	2.08021	43.468	4.0
43	4	2	-2	2.05793	43.963	1.0
44	2	4	1	2.02651	44.681	1.0
45	3	3	-3	2.00473	45.193	1.0

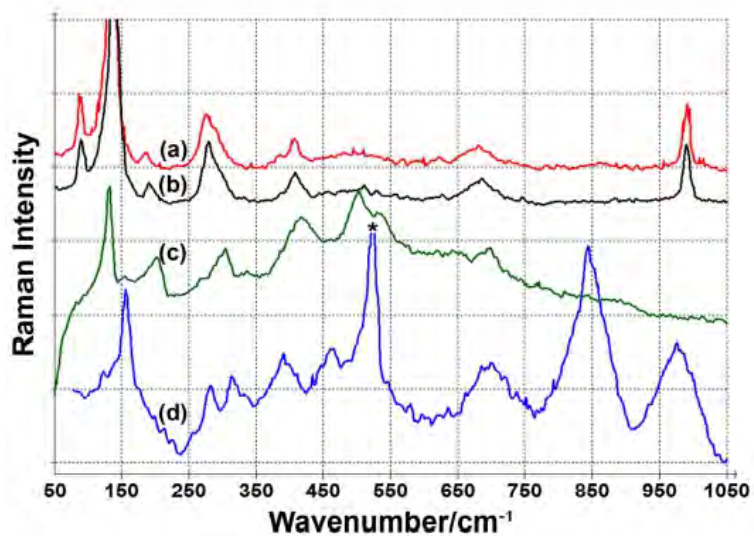
Stick Pattern



Appendix B

Raman scattering of V_6O_{13}

Raman scattering in V_6O_{13} has been reported for V_6O_{13} (a) a single crystal [24] and (b) microcrystalline powder [24, 25] which demonstrate the same response (Fig.4.2). For (c) and (d) are a magnetron sputtered film and a flash evaporated film, respectively.



Bibliography

- [1] How do thermochromic materials work? - explain that stuff. <https://www.explainthatstuff.com/thermochromic-materials.html>. (Accessed on 04/24/2021).
- [2] M. Li, S. Magdassi, Y. Gao, and Yi Long. Hydrothermal synthesis of VO_2 polymorphs: advantages, challenges and prospects for the application of energy efficient smart windows. *Small*, 13(36):1701147, 2017.
- [3] Z. Cao, X. Xiao, X. Lu, Y. Zhan, H. Cheng, and G. Xu. A simple and low-cost combustion method to prepare monoclinic VO_2 with superior thermochromic properties. *Scientific reports*, 6(1):1–9, 2016.
- [4] W. Zeng, N. Chen, and W. Xie. Research progress on the preparation methods for VO_2 nanoparticles and their application in smart windows. *CrystEngComm*, 22(5):851–869, 2020.
- [5] L. Kang, Y. Gao, and H. Luo. A novel solution process for the synthesis of VO_2 thin films with excellent thermochromic properties. *ACS applied materials & interfaces*, 1(10):2211–2218, 2009.
- [6] M. Demeter, M. Neumann, and W. Reichelt. Mixed-valence vanadium oxides studied by xps. *Surface Science*, 454:41–44, 2000.
- [7] Z. Yang, C. Ko, and S. Ramanathan. Oxide electronics utilizing ultrafast metal-insulator transitions. *Annual Review of Materials Research*, 41:337–367, 2011.
- [8] V. Eyert. The metal-insulator transitions of VO_2 : A band theoretical approach. *Annalen der Physik*, 11(9):650–704, 2002.
- [9] A. Cavalleri, Th. Dekorsy, HH. Chong, JC. Kieffer, and RW. Schoenlein. Evidence for a structurally-driven insulator-to-metal transition in VO_2 : A view from the ultrafast timescale. *Physical Review B*, 70(16):161102, 2004.

- [10] T. Yao, X. Zhang, Z. Sun, S. Liu, Y. Huang, Y. Xie, C. Wu, X. Yuan, W. Zhang, Z. Wu, et al. Understanding the nature of the kinetic process in a VO_2 metal-insulator transition. *Physical review letters*, 105(22):226405, 2010.
- [11] J. Nag, Richard F. Haglund Jr., E. Andrew P., and Karren L. More. Non-congruence of thermally driven structural and electronic transitions in VO_2 . *Journal of Applied Physics*, 112(10):103532, 2012.
- [12] TC. Koethe, Z. Hu, MW. Haverkort, C Schüßler-Langeheine, F Venturini, NB Brookes, Oscar Tjernberg, W Reichelt, HH Hsieh, H-J Lin, et al. Transfer of spectral weight and symmetry across the metal-insulator transition in VO_2 . *Physical review letters*, 97(11):116402, 2006.
- [13] J. Als-Nielsen and D. McMorrow. *Elements of modern X-ray physics*. John Wiley & Sons, 2011.
- [14] What is raman spectroscopy? | raman spectroscopy principle. <https://www.edinst.com/blog/what-is-raman-spectroscopy/>. (Accessed on 05/07/2021).
- [15] Theory of uv-visible spectroscopy (the basics) | jasco. <https://jascoinc.com/learning-center/theory/spectroscopy/uv-vis-spectroscopy/>. (Accessed on 04/24/2021).
- [16] X-ray diffractometer (xrd)-d8 advance from bruker : Quote, rfq, price and buy. <https://www.azomining.com/equipment-details.aspx?EquipID=779>. (Accessed on 04/26/2021).
- [17] Raman spectrometer-modular systems-horiba. <https://www.horiba.com/deu/products/detail/action/show/Product/raman-spectrometer-modular-systems-1694/>. (Accessed on 05/18/2021).
- [18] Resources-perkin-elmer lambda 900 uv-vis-nir spectrometer - bier research group - chemistry - carnegie mellon. http://www.chem.cmu.edu/groups/bier/procedure_files/uvvis.html. (Accessed on 04/24/2021).
- [19] C. Weeks, YN. Song, M. Suzuki, NA. Chernova, PY. Zavalij, and MS. Whittingham. The one dimensional chain structures of vanadyl glycolate and vanadyl acetate. *Journal of Materials Chemistry*, 13(6):1420–1423, 2003.
- [20] P. Shvets, O. Dikaya, K. Maksimova, and A. Goikhman. A review of raman spectroscopy of vanadium oxides. *Journal of Raman Spectroscopy*, 50(8):1226–1244, 2019.

- [21] W. Li, S. Ji, Y. Li, A. Huang, H. Luo, and P. Jin. Synthesis of VO_2 nanoparticles by a hydrothermal-assisted homogeneous precipitation approach for thermochromic applications. *Rsc Advances*, 4(25):13026–13033, 2014.
- [22] C. Julien, G.A. Nazri, and O. Bergström. Raman scattering studies of microcrystalline VO_{13} . *Physica Status Solidi B Basic Research*, 201(1):319–326, 1997.
- [23] H. Zhang, X. Xiao, X. Lu, G. Chai, Y. Sun, Y. Zhan, and Gang Xu. A cost-effective method to fabricate VO_2 (m) nanoparticles and films with excellent thermochromic properties. *Journal of Alloys and Compounds*, 636:106–112, 2015.
- [24] J. Höwing, T. Gustafsson, and J. Thomas. Low-temperature structure of VO_{13} . *Acta Crystallographica Section B: Structural Science*, 59(6):747–752, 2003.
- [25] XJ. Wang, HD. Li, YJ. Fei, X. Wang, YY. Xiong, YX. Nie, and KA. Feng. Xrd and raman study of vanadium oxide thin films deposited on fused silica substrates by rf magnetron sputtering. *Applied Surface Science*, 177(1-2):8–14, 2001.